RIS-Assisted Beamforming Optimization Based on DNN in the UAV-ISAC System

Zhiyu Liu[1[0009−0004−3039−7763]], Jieling Zhang[1[0009−0006−8024−4022]], Bin Yang[1],*[0000−0003−3322−867X], Pinlong Zhao[1[0000−0002−3161−5003]], Pengfei Jiao[1[0000−0003−1049−1002]], Zhidong Zhao[1[0000−0001−6659−3732]], and Huaming Wu[2[0000−0002−4761−9973]]

[1] School of Cyberspace, Hangzhou Dianzi University, Hangzhou 310018, China
[2] Center for Applied Mathematics, Tianjin University, Tianjin 300072, China

Abstract. Integrated sensing and communication (ISAC), as a key technology for 6G communication, alleviates frequency spectrum pressure by enabling communication and sensing to share the same hardware platform and frequency spectrum resources. However, high-frequency signals exhibit weak penetration capabilities. Particularly in non-line-of-sight (NLoS) scenarios where obstacles exist between the transmitter and receiver, the performance of communication and sensing sharply decline. To solve this problem, reconfigurable intelligent surface (RIS) has been widely studied for its ability to improve signal attenuation and communication environment. This paper constructs a new channel model using unmanned aerial vehicles (UAV) equipped with RIS to solve the problem of NLoS communication faced by ISAC systems. The beamforming weights of base station (BS) and phase shift of RIS are jointly optimized by deep neural network (DNN), so as to maximize the user's communication sum rate and sensing effect on sensing target. Simulation results demonstrate the algorithm proposed in this paper, namely ISAC-Aerial RIS-DNN (IARD), is effective for NLoS communication and achieve higher sum rate.

Keywords: RIS · ISAC · UAV · wireless communication · DNN

1 Introduction

With 5G moving towards a new era of everything, traffic density and connection scale are surging, and the world is stepping up 6G research. ISAC technology is widely regarded as one of the core enabling technologies for 6G systems [12] [6]. It converges wireless communication and radar sensing functionalities onto a unified hardware platform, enabling resource sharing and coordinated operation between these capabilities. This integration simultaneously addresses the demands for high-data-rate communications and high-precision environmental sensing while alleviating spectrum scarcity issues. However, how to ensure signal transmission stability and perception accuracy in complex wireless channel environment is still an important challenge.

To address these challenges, RIS, as an innovative electromagnetic reconfigurable architecture, has become a key technology for next-generation ISAC systems. RIS dynamically modulates electromagnetic waves through programmable units to enhance communication reliability and perception resolution. In non-line-of-sight(NLoS) environments, RIS establishes artificial LoS links through intelligent reflections to avoid obstacles, enhance target detection capabilities, and mitigate path loss [13] [2] [14]. In addition, RIS-assisted beamforming optimizes resource allocation, maximizes signal-to-noise ratio(SNR) and improves detection probability [11] [7] [1]. RIS-equipped UAVs play a key role in the construction of an integrated air, space and sea network. Its flexible deployment capability and three-dimensional mobility support the intelligent networking of space communication nodes, effectively solving problems such as signal fading and incomplete coverage [15] [4], realizing reliable and comprehensive network coverage, and contributing to the construction of an efficient communications infrastructure.

The current joint optimization methods for BS beamforming and RIS phase shift in UAV-carried RIS communication sensing integrated systems are mainly classified into traditional and deep learning methods. For example, Zhou et al. [18] use genetic and greedy algorithms to optimize the beamforming and RIS reflection unit phases to maximize the multiuser rate. Although the traditional methods are effective, they require large computational resources and are prone to produce suboptimal solutions. In contrast, deep learning methods have made significant progress in RIS optimization, and DNN can automatically learn complex nonlinear mapping relations from a large amount of data without relying on artificially designed heuristic rules, and exhibits stronger adaptability and generalization ability when dealing with high-dimensional nonlinear problems. In addition, DNN is fast in reasoning after training, which is especially suitable for scenarios with high real-time requirements [5].

This paper proposes a joint optimization method for BS beamforming and RIS phase shifts based on DNN, targeting an ISAC system utilizing an UAV-mounted RIS. In complex urban environments, buildings may obstruct the LoS link between the UAV and ground users, severely degrading channel quality. To circumvent these obstructions and enhance signal coverage, we deploy the RIS on the UAV platform. Building upon this configuration, we establish a RIS-assisted UAV-ISAC system model. Finally, a DNN-based algorithm is designed to jointly optimize the BS beamforming matrix and the RIS phase shift configuration. This approach aims to significantly improve signal transmission quality and effectively enhance the integrated communication and sensing performance of the system under challenging environmental conditions. The main contributions of this paper are as follows:

– First, we innovatively propose a model that fuses ISAC, RIS, and UAV to improve communication and sensing capabilities in complex environments. Specifically, this paper proposes a RIS-assisted ISAC system to improve the stability of signal transmission and the accuracy of perception in complex wireless channel environments. Meanwhile, in order to reduce the signal in-

terference from ground objects, NLoS links are constructed by mounting RIS on UAV to extend the coverage of communication and sensing.
– Next, the sensing sum rate is incorporated as a penalty term into the integrated rate objective function to facilitate the joint optimization of both communication rate and sensing sum rate. Leveraging the capability of DNN to characterize high-dimensional nonlinear relationships, alongside the end-to-end collaborative optimization mechanism which mitigates convergence to local optima, is anticipated to yield enhanced performance advantages.
– Finally, we conduct comprehensive simulation experiments under the modeled scenarios to validate the effectiveness of the proposed model and its associated algorithms. The results show that the IARD algorithm consistently achieves a higher achievable sum rate compared to several baseline methods across diverse experimental settings, demonstrating a clear performance advantage. Moreover, the proposed methodology exhibits strong robustness, maintaining stable and competitive performance under varying learning rates, which underscores its practical reliability and adaptability in different configurations.

2 System Model And Problem Formulation

2.1 Scene Description

As shown in Fig. 1, this paper investigates a BS utilizing a downlink RIS-assisted UAV multi-input single-output network. In this system, the BS is equipped with M wire lines to provide service to K single antenna users sensing a sensed target. The lifted UAV carrying RIS's acts as a relay node to provide additional connectivity to the users. The UAV is equipped with a RIS module containing N passive phase-shifting elements, which are flexibly assisted by adjusting the position of the UAV and the phase-shifting settings of the RIS. Ground obstacles are assumed to be impenetrable, so the communication link between the BS and the users is not considered. K ground users can only communicate with the BS through the RIS on the UAV, and the sensing target is sensed by the BS through the RIS on the UAV. A 3D Cartesian coordinate system is constructed with the BS as the coordinate origin, i.e., the BS coordinates are $(0, 0, 0)$. All users are located on the ground, i.e., their vertical coordinates are 0. Assuming that the UAV knows the location of each user, the link channel information between the UAV and each user can be determined accordingly. The UAV flies at height z and assists each user with its communication process with the BS. The coordinates of the UAV are (x, y, z) and the coordinates of the users are $(a, b, 0)$.

2.2 Channel Model

Since the RIS carried by the UAV is deployed in the air, the link from the BS to the RIS is mainly a LoS path. In the case of the free space path loss model, the Downlink Channel matrix from the BS to the RIS is:

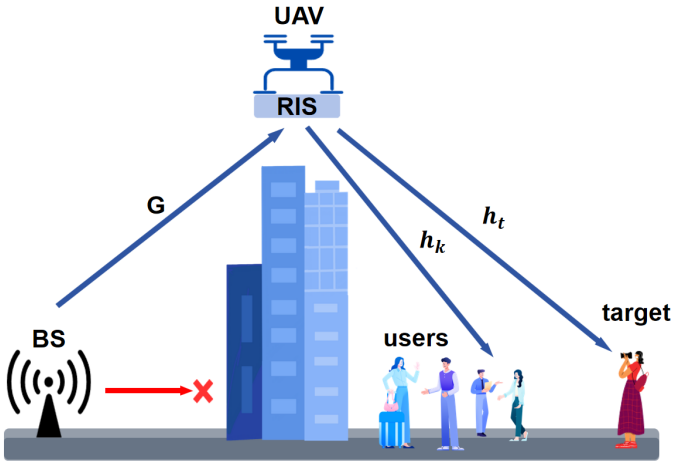

Fig. 1. Scene Model

$$\mathbf{G} = \sqrt{\gamma D_0^{-2}}\mathbf{a}_B\left(\phi_{BS}^A\right)\mathbf{a}_R\left(\phi_{RIS}^A, \phi_{RIS}^E\right)^H, \tag{1}$$

where D_0 is the distance from the BS to the low-altitude RIS, and the channel gain at the reference distance $D = 1$ m is denoted as γ. $\mathbf{a}_R\left(\phi_{RIS}^A, \phi_{RIS}^E\right)$is the receiving array response vector at the low-altitude RIS. ϕ_{RIS}^A and ϕ_{RIS}^E are the azimuth and elevation angles of the arrival angle, respectively. $\mathbf{a}_B\left(\phi_{BS}^A\right)$ denotes the response vector of the transmit array in BS. ϕ_{BS}^A is the azimuth of the departure angle. $(\cdot)^H$ denotes the conjugate transpose operator. Assuming that the low-altitude RIS elements are arranged in a uniform square array, the receiver array response vector $\mathbf{a}_R\left(\phi_{RIS}^A, \phi_{RIS}^E\right)$ of the RIS can be expressed as:

$$\begin{aligned}\mathbf{a}_R\left(\phi_{RIS}^A, \phi_{RIS}^E\right) = \sqrt{\frac{1}{N}} \cdot \Big[1, e^{2\pi k \frac{d_n}{\lambda}(af(\phi)g(\phi)+bf(\phi))}, \\ \ldots, e^{2\pi k \frac{(N-1)d_n}{\lambda}(f(\phi)g(\phi)+f(\phi))}\Big]^T,\end{aligned} \tag{2}$$

where $d_n = \lambda/2$ is the distance between two neighboring elements in the RIS and λ is the wavelength. $f(\phi) = \sin(\phi_{RIS}^A)$, $g(\phi) = \cos(\phi_{RIS}^E)$. The Downlink Channel vector h_k between the RIS and the user k can be expressed as:

$$\mathbf{h}_k = \sqrt{\gamma D_k^{-2}}\mathbf{a}_T\left(\phi_{RIS}^{A_k}, \phi_{RIS}^{E_k}\right), \tag{3}$$

where D_k is the distance between the RIS and the kth user. $\mathbf{a}_T\left(\phi_{RIS}^{A_k}, \phi_{RIS}^{E_k}\right)$ is the transmitting array response vector at the RIS. The Downlink Channel vector $\mathbf{h}_t$ between the RIS and the target can be expressed as:

$$\mathbf{h}_t = \sqrt{\gamma D_t^{-2}}\mathbf{a}_T\left(\phi_{RIS}^{A_{tar}}, \phi_{RIS}^{E_{tar}}\right), \tag{4}$$

where D_t is the distance from the RIS to the target. $\mathbf{a}_T\left(\phi_{RIS}^{A_{tar}}, \phi_{RIS}^{E_{tar}}\right)$is the response vector of the transmit array from RIS to target.

2.3 Signal Model

In this paper, we denote the Downlink Channel matrix transmitted from the BS to the RIS by $\mathbf{G} \in C^{M\times N}$, and the Downlink Channel vector reflected from the RIS to user k by $\mathbf{h}_k \in C^{N\times 1}$. It is assumed that the channel obeys a Rice distribution and the channel is a Rayleigh fading channel gain. Therefore, the signal received at each user can be expressed as:

$$\begin{aligned} y_k &= \left(\mathbf{G}\mathbf{diag}(\boldsymbol{\theta})\mathbf{h}_k\right)^T \mathbf{x} + n_k, \\ &= \mathbf{U}_k^T \mathbf{x} + n_k, \end{aligned} \tag{5}$$

where $(\cdot)^T$ denotes the transpose operator. $\mathbf{diag}(\boldsymbol{\theta})$ is the diagonal matrix of the vector $\boldsymbol{\theta}$ on the main diagonal. $\mathbf{U}_k = \mathbf{G}\mathbf{diag}(\boldsymbol{\theta})\mathbf{h}_k$ denotes the relationship between the BS and the user k the cascade channel between BS and user via RIS. $n_k \sim \mathcal{CN}(0, \sigma_k^2)$ denotes the additive white Gaussian noise. $\boldsymbol{\theta} = [\boldsymbol{\theta}_1, \cdots, \boldsymbol{\theta}_N]^T$ denotes the reflection coefficient of RIS. $\mathbf{x} = \mathbf{B}_c\mathbf{S}_c + \mathbf{B}_t\mathbf{S}_t = \mathbf{B}\cdot\mathbf{S}$ is the transmit signal at BS for all users k, which consists of the source signal and the BS beamforming vector $\mathbf{b}_k$, $\mathbf{B} = [\mathbf{b}_1, \ldots, \mathbf{b}_K, \mathbf{b}_t]$ and $S = [s_1, \ldots, s_K, s_t]^T$, $\mathbb{E}\left[ss^H\right] = I$. The signal to interference plus noise ratio (SINR) of user k can be described as :

$$\xi_k = \frac{\left|\mathbf{U}_k^H \mathbf{b}_k\right|^2}{\sum_{j=1, j\neq k}^{K} \left|\mathbf{U}_k^H \mathbf{b}_j\right|^2 + \sigma_k^2}. \tag{6}$$

Sensing is performed on a sensing target. When sensing at the BS, the transmitted signal has to arrive at the target through the reflective link of RIS. Then it is folded back to the BS from the target through the reflective link of RIS, so the echo signal reflected back from the sensing target can be expressed as:

$$\begin{aligned} \mathbf{y}_t &= \eta_t \left(\mathbf{G}\mathbf{diag}(\boldsymbol{\theta})\mathbf{h}_t\right)\left(\mathbf{G}\mathbf{diag}(\boldsymbol{\theta})\mathbf{h}_t\right)^T \mathbf{x} + \mathbf{n}_t, \\ &= \eta_t \mathbf{U}_t \mathbf{U}_t^T \mathbf{x} + \mathbf{n}_t, \end{aligned} \tag{7}$$

where $n_t \sim \mathcal{CN}(0, \sigma_t^2)$ denotes the additive white Gaussian noise. $\eta_t \sim \mathcal{CN}(0, \sigma_r^2)$ denotes the radar cross section(RCS). Assuming that the radar signal is not interfered by the communication user's signal, the expression for the radar SNR is [8]:

$$\xi_t = \frac{\eta_t \left|\mathbf{b}_t^H \mathbf{U}_t \mathbf{U}_t^H \mathbf{b}_t\right|^2}{\sigma_t^2}. \tag{8}$$

For a user, the sum rate from BS to user $k(k = 1, 2, 3, ...K)$ can be expressed as:

$$R_k = \log_2\left(1 + \xi_k\right). \tag{9}$$

For the target, this paper uses a penalty term to make the sensing sum rate join the total sum rate. Where $\eta(\eta > 0)$ is a threshold value for whether the penalty is enforced or not. If the sensing sum rate is less than η, the penalty is enforced. Conversely, if the sensing sum rate is greater than η , then the sum rate increases. And μ represents the severity of the punishment. The expression for the sensing sum rate is as follows:

$$R_t = \mu \cdot \left(\log_2\left(1 + \xi_t\right) - \eta\right), \tag{10}$$

The ultimate goal of this paper is to maximize the sum rate of K users and sensed targets by jointly optimizing the BS beamforming and RIS reflection coefficients while satisfying the BS transmit power constraints and RIS phase shift constraints. Therefore, the optimization problem in this paper is formulated as:

$$\underset{b_k,\theta}{max} \sum_{k=1}^{K} R_k + R_t, \tag{11a}$$

$$\text{s.t. } \mathbb{E}\left[\|\boldsymbol{x}\|^2\right] \leq P_{\max}, \tag{11b}$$

$$\boldsymbol{\theta} \in \boldsymbol{\Theta}^N, \tag{11c}$$

where P_{max} denotes the maximum transmit power of the BS. (11b) equation denotes the transmit power constraint of the BS. (11c) equation denotes the finite resolution (B bits) RIS phase constraint, with discrete phase shifts $\boldsymbol{\Theta} = \left\{ \mathrm{e}^{\mathrm{k}\varphi_{\mathrm{n}}} \middle| \varphi_n \in \left\{ 0, \frac{2\pi}{2^\beta}, \ldots, \frac{2\pi\left(2^\beta - 1\right)}{2^\beta} \right\} \right\}$.

3 DNN-Based Joint Optimization of Beamforming and Phase Shift Matrix

A feed-forward fully connected DNN is essentially a multilayer perceptual machine containing multiple hidden layers. The DNN is divided by the location of different layers and the internal neural network layers can be categorized into three types, input, hidden and output layers. The nodes in neighboring layers are fully connected, while there is no connection between nodes in the same layer. The activation values of hidden layer nodes are obtained by applying a nonlinear activation function to the linearly weighted sum of the activation values from the previous layer and the weights of the current network layer. For a DNN containing L hidden layers [9] [10]. Assuming that the input is $\mathbf{h}^0 = \mathrm{X}$, the calculation of the activation value of the hidden layer can be expressed by the following equation:

$$\mathbf{a}^l = \mathbf{W}^l \mathbf{h}^{l-1} + \mathbf{b}^l \quad (1 \leq l \leq L+1), \tag{12a}$$

$$\mathbf{h}^{l-1} = f\left(\mathbf{a}^l\right) \quad (1 \leq l \leq L), \tag{12b}$$

where $\mathbf{W}^l$ and $\mathbf{b}^l$ represent the weights and bias vectors of the lth layer of the network, respectively. $f(\cdot)$ denotes the nonlinear activation function of the hidden layer nodes.

To optimize the network parameters, backpropagation is employed as the foundational learning mechanism. In this phase, the error is propagated backward from the output layer through each hidden layer. The gradients of the loss function with respect to all weights and biases are computed efficiently using the chain rule. These gradients are then used to update the parameters via gradient-based optimization algorithms, thereby minimizing the prediction error and enhancing model accuracy. Through this iterative process, the DNN progressively refines its internal representations and improves its performance on the given task.

IARD Algorithm

Input: Cascaded channel $\mathbf{U_k}$ between BS and user k via RIS and cascaded channel between BS and target $\mathbf{U_t}$.

Training Phase

Initialize: Extract relevant information from $\mathbf{U_k}, \mathbf{U_t}$ to initialize user nodes and RIS nodes: $\boldsymbol{\theta}$, $\mathbf{B}$ (beamforming matrix) $\leftarrow \mathbf{U_k}, \mathbf{U_t}$.
for iteration t **do**
  Use mini-batch training samples.
  for DNN training layer d **do**
    PhaseNet: Compute phase shift matrix $\boldsymbol{\theta}$.
    Compute equivalent channel: $\mathbf{B}_{\text{eff}} = H \cdot \boldsymbol{\theta}$.
    BeamNet: Generate $\mathbf{B}$ based on $\mathbf{B}_{\text{eff}}$.
  end for
  Compute batch loss:

$$L = -\sum_{k=1}^{K} \log_2 (1 + \xi_k) - \mu \cdot (\log_2 (1 + \xi_t) - \eta)$$

  Backpropagation: Update network parameters via gradient descent:

$$\mathbf{B}_l^{(t+1)} = \mathbf{B}_l^{(t)} - \eta \nabla_{\mathbf{B}_l} L$$

end for

Output: Beamforming matrix $\mathbf{B}$ at BS and phase shift matrix θ at RIS.

3.1 Input Layer

At this layer, the real and imaginary components of the cascaded channel state information $R_k \in C^{M \times N \times K}$ are reorganized into a $2D$ tensor of $2K$ channels, which allows the network to learn both real and imaginary information to obtain more complete channel characteristics.

3.2 PhaseNet Design

The main task of the phase control sub-network is to generate the RIS phase shift matrix $\boldsymbol{\theta}$, i.e. to optimize the signal propagation path by controlling the phase. The network learns how to adjust the phase to optimize the signal transmission by performing feature extraction through a multilayer convolutional neural network and a fully connected layer. Since neural networks can usually only handle real data, but each element of the input sample is a complex number. So it needs to be converted to real numbers. In this paper, we use independent channels to extract the real and imaginary parts separately [16], forming $2K$ channels. The input sample dimension becomes $R^{batchsize \times 2K \times M \times N}$. The samples are processed by the neural network and output. The output phase matrix is normalized to ensure that it satisfies the unit mode constraints. Finally, the normalized phase matrix is obtained. The specific steps are shown in Flg.2.

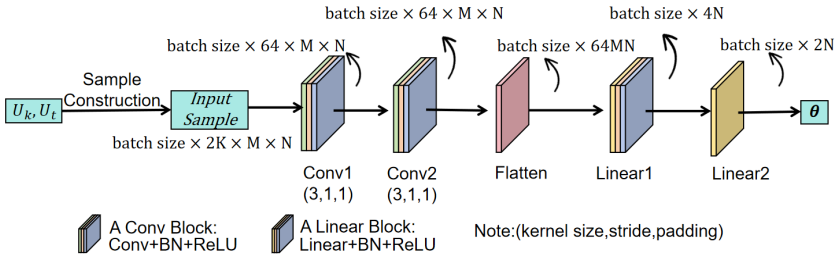

Fig. 2. Network Architecture of PhaseNet

3.3 BeamNet Design

The purpose of the beamforming subnetwork is to generate a BS beamforming matrix based on the input channel state information to optimize signal reception and transmission. The subnetwork uses a fully connected layer to perform further feature learning on the input channel information and outputs the BS beamforming matrix $\mathbf{B}$. For the input samples, an equivalent channel needs to be constructed for input to the beamforming subnetwork. First, it is necessary to extract each user's channel from the joint channels $\mathbf{U_k}$ and $\mathbf{U_t}$. The complex channel is divided into real and imaginary parts and the augmented real-valued matrix is constructed to preserve the complex multiplicative relationship. Then, the phase-adjusted equivalent channel is computed by combining the phase parameter $\boldsymbol{\theta}$ with the channel matrix by matrix multiplication. Finally, the equivalent channels of all users are spliced along the feature dimensions to form the $R^{batchsize \times 2MK}$ equivalent channel. The beamforming matrix is obtained after subnetwork processing and normalized to make it satisfy the maximum power constraint. Finally the normalized beamforming matrix is obtained. The specific steps are shown in Fig.3.

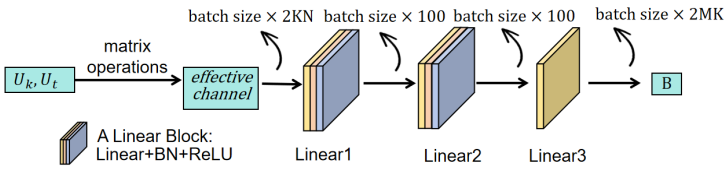

Fig. 3. Network Architecture of BeamNet

4 Experimentation and Analysis

4.1 Parameter Setting

In this section, simulation results are presented to validate the effectiveness of the proposed joint optimization algorithm for BS beamforming and RIS phase shift design. Following the system configurations adopted in [19] and [3], the BS is equipped with 8 antennas to serve 4 single-antenna users. The UAV is integrated with a RIS comprising 50 passive reflecting elements. Users and sensing target locations are randomly distributed within a circular region centered at $(200, 0, 0)$ with a radius of 10 meters, simulating a typical deployment scenario containing both communication users and a sensing object of interest. The maximum transmit power at the BS is set to $P_{\max} = 10mW$, and the path loss exponent is set to $\beta = 2$. For the DNN training configuration, the Adam optimizer is employed for weight updates, with an initial learning rate of 0.001 and a decay rate of $1e-6$. The penalty coefficients μ and η are empirically chosen as 0.8 and 0.1, respectively, through systematic hyperparameter tuning to maximize the sum-rate performance.

Table 1. Experimental Parameters

Parameter	**Value**
Number of BS antennas	8
Number of RIS elements	50
Maximum transmit power	10 mW
Path loss exponent	2
Penalty item coefficient μ	0.8
Penalty item coefficient η	0.1
Number of users	4
Batch size	64
Learning rate	0.001
Learning rate decay factor	1×10^{-6}
Number of convolutional layers	2
Number of neurons	564

The following approaches are compared:

1. IARD model proposed in this paper;
2. IARD-$\boldsymbol{\theta}$-non-opt: randomly generating the RIS reflection coefficients $\boldsymbol{\theta}$, and the DNN optimizes only the BS beamforming matrix;
3. ISAC-Aerial RIS (IAR)-GLS: based on the principle of the greedy local search algorithm proposed in Paper [17], the model of this paper is modified to optimize the RIS reflection phase shift and beamforming matrix using the greedy local search algorithm;
4. IAR-random-$\boldsymbol{\theta}$-$\mathbf{B}$: random generation of RIS reflection coefficients $\boldsymbol{\theta}$ and beamforming matrix $\mathbf{B}$.

4.2 Maximum Sum Rate

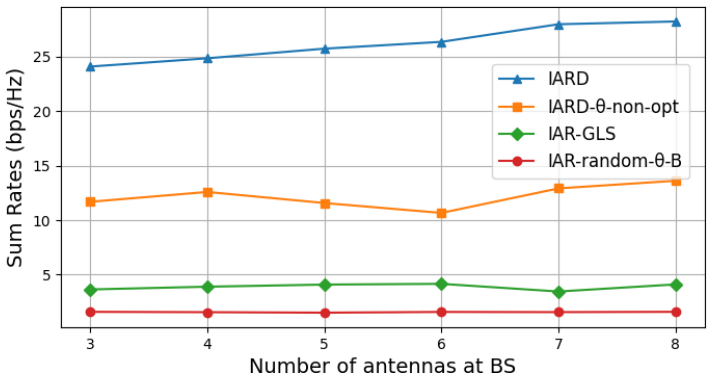

Fig. 4. Maximum sum rate plotted against antennas

Fig. 4. illustrates the user communication and sensing sum rate versus the number of BS antennas. The number of RIS reflective elements in the experiment is fixed at 50. For the evaluated scenarios, the sum rate of IARD is the highest for all numbers of BS antennas. For the sum rate, IARD is stabilized at $26.22bps/Hz$. IARD-$\boldsymbol{\theta}$-non-opt is stabilized at $12.18bps/Hz$. IAR-GLS is stable at $3.89bps/Hz$. IAR-random-$\boldsymbol{\theta}$-$\mathbf{B}$ is stable at $1.56bps/Hz$. The experimental results show that the performance of the proposed IARD scheme is significantly improved compared to all three baseline methods under the joint optimization conditions.A RIS optimizes signal propagation by adjusting the electromagnetic properties (e.g., reflection phase) of its surface units. This process is completely controlled by the RIS itself, independent of how many antennas are used by the BS. Instead, the BS focuses the signal energy in a specific direction by adjusting the signal strength (amplitude) and phase difference of each antenna in the antenna array. Even though the accuracy of the beam is reduced with a smaller number of antennas in the BS, it can still be tuned algorithmically to achieve basic directional functionality. The fundamental mechanism of beamforming relies

on coherent signal superposition across antenna elements to control radiation directionality, rather than the mere quantity of antennas. Therefore, the number of antennas at the BS has relatively little effect on the experimental results.

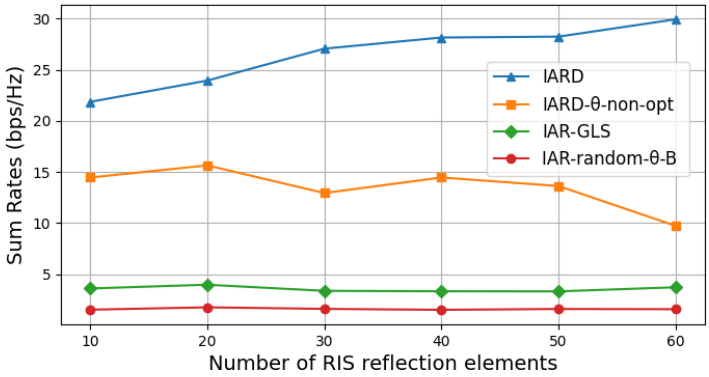

Fig. 5. Maximum sum rate plotted against RIS elements

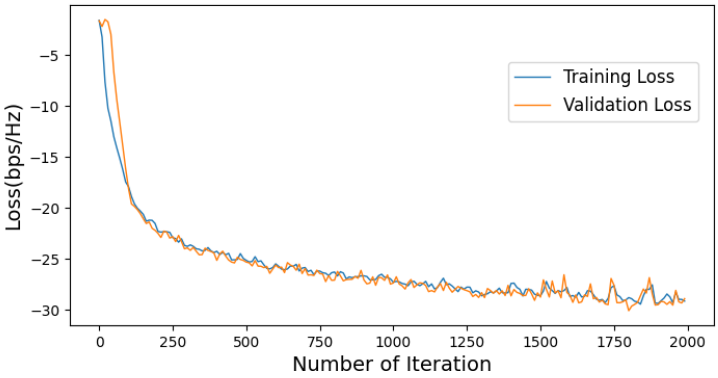

Fig. 6. Maximum sum rate plotted against learning rate

Fig. 5. illustrates the user communication and sensing sum rate versus the number of RIS reflection elements. The number of BS wires in the experiment is fixed at 8. The maximum sum rate is changed by varying the number of RIS reflective elements, while the IARD has the highest sum rate for all of them. For the maximum sum rate, IARD is stabilized at $26.54bps/Hz$, IARD-$\boldsymbol{\theta}$-non-opt is stabilized at $13.47bps/Hz$. IAR-GLS is stable at $3.58bps/Hz$. IAR-random-$\boldsymbol{\theta}$-**B**

is stable at $1.58bps/Hz$. The experimental results show that the performance of the proposed IARD scheme is significantly improved compared to all three baseline methods under the joint optimization conditions. The performance and flexibility of the RIS are significantly affected by the number of its reflection units. The number of reflection units directly determines the phase adjustment accuracy of RIS. RIS beamforming precision scales with the number of programmable elements, with higher element counts enabling sharper beam control and consequently greater system throughput. In addition, more reflection units means a larger effective reflection area, which not only enhances the incident signal capture capability, but also significantly improves the reflected signal strength through the array gain. Particularly in millimeter-wave and other high-frequency regimes, large-scale RIS can effectively compensate for propagation path loss through coherent phase manipulation.

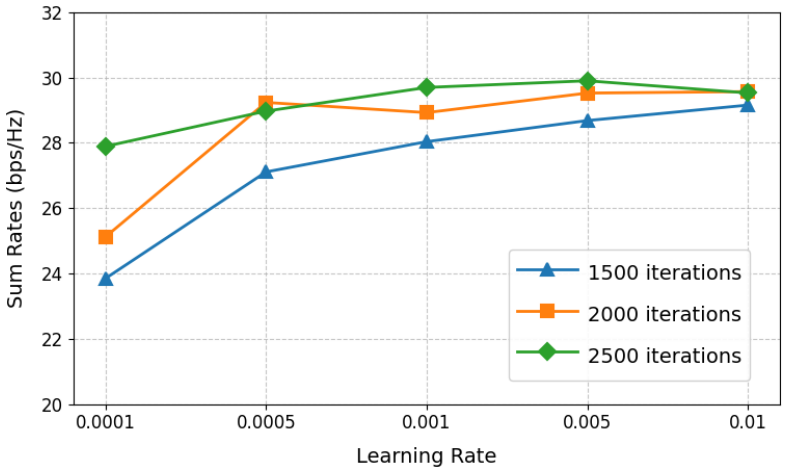

Fig. 7. Maximum sum rate plotted against learning rate

As shown in Fig.6, to demonstrate model convergence, we plotted the loss against the number of iterations. As shown in the figure, the loss stabilizes and plateaus beyond a certain number of iterations, indicating that the model has successfully converged.

4.3 Algorithm Robustness Analysis

To demonstrate the robustness of the IARD algorithm, we set up several sets of comparison experiments. By adjusting the learning rate and the number of iteration rounds, the relationship between the learning rate and the optimiza-

tion results in the case of different number of iteration rounds is obtained. The experimental results are shown in Fig. 7.

The experimental results show that, with the same number of iteration rounds, the difference of the maximum sum rate obtained by optimization with different learning rates does not exceed 15.1%. In addition, the maximum sum rate obtained by optimization does not change significantly with the change of iteration rounds. This shows that the IARD algorithm converges well and is robust.

5 Conclusion

This paper proposes a UAV-carried RIS-assisted ISAC system to address user communication and sensing SNR degradation caused by LoS blockage in dense obstacle environments. Through the joint optimization of BS beamforming and RIS phase-shift configurations, significant improvements in user sum rate are achieved. Specifically, the IARD framework is employed to optimize both the BS beamforming and RIS phase shifts in our experimental simulations. The results demonstrate that the proposed IARD model offers substantial advantages in sum-rate performance and exhibits stronger optimization capabilities compared to traditional heuristic algorithms. Furthermore, by incorporating the sensing SNR as a penalty term into the sum-rate objective, this work successfully enables the co-optimization of communication and sensing performance. Additional experiments also confirm that the IARD model maintains stable performance under varying learning rates, indicating strong robustness. Despite these promising results, it should be noted that the current study is conducted under relatively ideal assumptions. Consequently, the practical applicability of the system in real-world scenarios remains to be further validated. Future work will focus on evaluating the performance under more realistic conditions, including dynamic obstacles, diverse environmental interference, and more complex mobility patterns.

References

1. Di Renzo, M., Zappone, A., Debbah, M., Alouini, M.S., Yuen, C., de Rosny, J., Tretyakov, S.: Smart radio environments empowered by reconfigurable intelligent surfaces: How it works, state of research, and the road ahead. IEEE Journal on Selected Areas in Communications **38**(11), 2450–2525 (2020). https://doi.org/10.1109/JSAC.2020.3007211
2. ElMossallamy, M.A., Zhang, H., Song, L., Seddik, K.G., Han, Z., Li, G.Y.: Reconfigurable intelligent surfaces for wireless communications: Principles, challenges, and opportunities. IEEE Transactions on Cognitive Communications and Networking **6**(3), 990–1002 (2020). https://doi.org/10.1109/TCCN.2020.2992604
3. Gao, J., Zhong, C., Chen, X., Lin, H., Zhang, Z.: Unsupervised learning for passive beamforming. IEEE Communications Letters **24**(5), 1052–1056 (2020). https://doi.org/10.1109/LCOMM.2020.2965532

4. Gu, X., Zhang, G.: A survey on uav-assisted wireless communications: Recent advances and future trends. Computer Communications **208**, 44–78 (2023). https://doi.org/https://doi.org/10.1016/j.comcom.2023.05.013, https://www.sciencedirect.com/science/article/pii/S0140366423001743
5. Li, M., Li, H.: Application of deep neural network and deep reinforcement learning in wireless communication. Plos one **15**(7), e0235447 (2020)
6. Liu, F., Cui, Y., Masouros, C., Xu, J., Han, T.X., Eldar, Y.C., Buzzi, S.: Integrated sensing and communications: Toward dual-functional wireless networks for 6g and beyond. IEEE Journal on Selected Areas in Communications **40**(6), 1728–1767 (2022). https://doi.org/10.1109/JSAC.2022.3156632
7. Liu, F., Zheng, L., Cui, Y., Masouros, C., Petropulu, A.P., Griffiths, H., Eldar, Y.C.: Seventy years of radar and communications: The road from separation to integration. IEEE Signal Processing Magazine **40**(5), 106–121 (2023). https://doi.org/10.1109/MSP.2023.3272881
8. Liu, R., Li, M., Liu, Q., Swindlehurst, A.L.: Snr/crb-constrained joint beamforming and reflection designs for ris-isac systems. IEEE Transactions on Wireless Communications **23**(7), 7456–7470 (2023)
9. Liu, W., Wang, Z., Liu, X., Zeng, N., Liu, Y., Alsaadi, F.E.: A survey of deep neural network architectures and their applications. Neurocomputing **234**, 11–26 (2017). https://doi.org/https://doi.org/10.1016/j.neucom.2016.12.038, https://www.sciencedirect.com/science/article/pii/S0925231216315533
10. Montavon, G., Samek, W., Müller, K.R.: Methods for interpreting and understanding deep neural networks. Digital Signal Processing **73**, 1–15 (2018). https://doi.org/https://doi.org/10.1016/j.dsp.2017.10.011, https://www.sciencedirect.com/science/article/pii/S1051200417302385
11. Nadeem, Q.U.A., Kammoun, A., Chaaban, A., Debbah, M., Alouini, M.S.: Asymptotic max-min sinr analysis of reconfigurable intelligent surface assisted miso systems. IEEE Transactions on Wireless Communications **19**(12), 7748–7764 (2020). https://doi.org/10.1109/TWC.2020.2986438
12. Wei, Z., Qu, H., Wang, Y., Yuan, X., Wu, H., Du, Y., Han, K., Zhang, N., Feng, Z.: Integrated sensing and communication signals toward 5g-a and 6g: A survey. IEEE Internet of Things Journal **10**(13), 11068–11092 (2023). https://doi.org/10.1109/JIOT.2023.3235618
13. Wu, Q., Zhang, R.: Towards smart and reconfigurable environment: Intelligent reflecting surface aided wireless network. IEEE Communications Magazine **58**(1), 106–112 (2020). https://doi.org/10.1109/MCOM.001.1900107
14. Wu, Q., Zhang, S., Zheng, B., You, C., Zhang, R.: Intelligent reflecting surface-aided wireless communications: A tutorial. IEEE Transactions on Communications **69**(5), 3313–3351 (2021). https://doi.org/10.1109/TCOMM.2021.3051897
15. Yang, L., Meng, F., Zhang, J., Hasna, M.O., Renzo, M.D.: On the performance of ris-assisted dual-hop uav communication systems. IEEE Transactions on Vehicular Technology **69**(9), 10385–10390 (2020). https://doi.org/10.1109/TVT.2020.3004598
16. Ye, J., Huang, L., Chen, Z., Zhang, P., Rihan, M.: Unsupervised learning for joint beamforming design in ris-aided isac systems. IEEE Wireless Communications Letters **13**(8), 2100–2104 (2024). https://doi.org/10.1109/LWC.2024.3402235
17. Zhou, H., Erol-Kantarci, M., Liu, Y., Poor, H.V.: Heuristic algorithms for ris-assisted wireless networks: Exploring heuristic-aided machine learning. IEEE Wireless Communications **31**(4), 106–114 (2024). https://doi.org/10.1109/MWC.010.2300321

18. Zhou, H., Erol-Kantarci, M., Liu, Y., Poor, H.V.: A survey on model-based, heuristic, and machine learning optimization approaches in ris-aided wireless networks. IEEE Communications Surveys Tutorials **26**(2), 781–823 (2024). https://doi.org/10.1109/COMST.2023.3340099
19. Zhu, Y., Bo, Z., Li, M., Liu, Y., Liu, Q., Chang, Z., Hu, Y.: Deep reinforcement learning based joint active and passive beamforming design for ris-assisted miso systems. In: 2022 IEEE Wireless Communications and Networking Conference (WCNC). pp. 477–482 (2022). https://doi.org/10.1109/WCNC51071.2022.9771666